34th Annual International Conference of the IEEE EMBS
San Diego, California USA, 28 August - 1 September, 2012

Reduction of Current Density at Disk Electrode Periphery by Shaping Current Pulse Edges

Boshuo Wang, James. D. Weiland, Senior *Member IEEE*

***Abstract*— Previous studies reveal that the primary distribution of the current density is sharply enhanced at the edge of a disk electrode submerged into a semi-infinite space of conductive solution. The current enhancement will cause the double layer capacitance at the periphery of the electrode to be charged much faster compared to the center, and can also lead to severe corrosion at the edge. While several studies focused on the geometric design of the electrode to reduce this enhancement, we explore the feasibility of achieving similar effect by shaping the edges of the current input. The simulation uses finite element analysis software to solve the system of partial differential equations and results show that the edge enhancement could be greatly reduced without significantly changing the input efficacy of current and/or charge.**

***Index Terms*—Neural prosthesis, electrical stimulation, microelectrode, neural engineering, implantable devices**

I. Introduction

The commonly used disk electrode has been of research interest for a long time [1]-[6]. Newman's analytical solution has concluded that the electric field and thus current density are both sharply enhanced at the periphery of the electrode [1]. Calculation shows that in response to a current step input the primary current density distribution along the radial axis in cylindrical coordinates is

$$J_z(r,z)|_{z=0} = \frac{J_0}{2\sqrt{1-r^2/a^2}}, \quad (1)$$

where J_0 is the average current density and a is electrode radius.

In practice the edge enhancement will not reach infinity as in theory, but is nevertheless an evident phenomenon. It is detrimental to the electrode itself as the enhanced electric field will cause chemical reactions, especially irreversible ones, to occur and thus corrode the periphery. In biomedical applications, the enhanced current density may also cause damage to tissue and result in undesired localized stimulation. Several studies reported different approaches to reduce this undesired behavior, mostly by altering the electrode geometric design [4]-[6]. A segmented circular electrode in which current-leveling of the annular segments by different resistors resulted in a nonuniform potential profile that would in turn yield a more uniform current density profile [4]. Several groups discussed designs of recessing the metal electrode deeper into the substrate, therefore reducing the current density enhancement on the surface of the aperture [5], [6]. These methods require complicated design, especially hardware modification. They also did not take the double layer capacitance or Faradaic reactions into consideration. These two components of the electrode, especially the former, will cause the primary current profile to redistribute to a more uniform distribution [3], [7]-[9]. Cantrell et al. studied the behavior of current density redistribution under different non-rectangular stimulus waveforms with modeling and also in vitro, and showed modified potential waveform could reduce the peripheral current density without trading-off stimulation efficacy [10], [11]. However potential waveforms need to be calibrated for the amount of charge injection, and the pulse length varies much. Behrend et al. proposed but did not test an approach to achieve more uniform current density profiles by retarding the rising edge of the input current pulse [9], which are typically rapidly rising (less than 10 μs rise time). We choose to quantitatively examine this approach by utilizing the Finite Element Model (FEM), which provides significant convenience and flexibility. Only the double layer capacitance of the electrode was included, giving good approximation to a capacitive electrode.

II. Finite Element Model

A. Model Geometry

Utilizing the rotational symmetry, the disk electrode model is built in cylindrical coordinates (Fig. 1), which is implemented in a 2D axisymmetric model in COMSOL Multiphysics v4.2a with the AC/DC module (COMSOL, Burlington, MA). The metal disk of radius a is embedded within the infinite large insulator base, and its double layer capacitor is

$$C = \gamma \pi a^2, \quad (2)$$

with γ being the double layer capacitance per unit area.

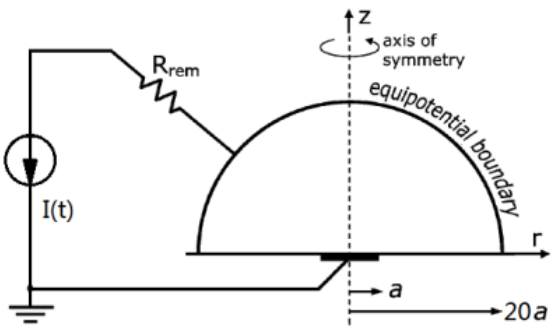

Figure 1. The metal electrode of radius a is positioned under the base of the hemispherical domain of resistive medium. The equipotential boundary and remaining resistance represent the rest of semi-infinite space. Ground is hold at disk for simulation but at infinity for data presentation

This material is based on work supported by the National Science Foundation under Grant No. EEC-0310723.

B. Wang is with the Biomedical Engineering Department, Viterbi School of Engineering, University of Southern California, Los Angeles, CA 90007 USA (e-mail: boshuowa@usc.edu).

J. D. Weiland is with the Ophthalmology Department, Keck School of Medicine, University of Southern California, Los Angeles, CA 90007 USA (e-mail: jweiland@usc.edu).

The theoretical resistance of the semi-infinite medium of conductivity κ above the electrode [1] and the corresponding time equivalent constant to that of a lumped RC circuit that characterizes the electrode are respectively given by

$$R_s = \frac{1}{4\kappa a}, \tag{3}$$

$$\tau = R_s C. \tag{4}$$

For simulation, the semi-infinite space is limited to a hemisphere with a radius equal to $20a$, and the resistance of the solution is therefore separated into two portions: distributed and lumped. The distributed region covers the simulation space from the electrode surface up to the approximately equipotential hemispherical boundary. The approximation introduces an error of $\pm 0.002\%$ in electric field magnitude on this surface [8]. The medium from here up to infinity is assumed to be equipotential at any radius, and the resistance is integrated into one lumped series resistance

$$R_{rem} = \frac{1}{2\pi\kappa}\left(\frac{1}{r_{min}} - \frac{1}{r_{max}}\right) = \frac{1}{40\pi\kappa a} \tag{5}$$

with $r_{min} = 20a$ and $r_{max} = +\infty$.

The mesh element size of the model is constrained to $a/30000$ on the disk boundary point, and is expanded by a growth factor of 1.1 towards the rest of solution space. This configuration achieves spatial resolution as well as minimum degree of freedom in the system [9].

B. System of Equations and Boundary Conditions

Laplace equation holds for the hemispheric simulation space and zero current density is enforced at the insulator base. The charging of the double layer at the electrode surface could be described with

$$\hat{n} \cdot \vec{J}(r,0,t)|_{r\le a} = \gamma \frac{\partial}{\partial t}\left(\phi(r,0,t)|_{r\le a} - \phi_{metal}(t)\right), \tag{6}$$

which is implemented as distributed impedance on the electrode surface in COMSOL. This module requires a reference potential. Therefore for the convenience of setting up the model, the potential at the electrode is considered as reference and held constant at ground

$$\phi_{metal}(t) \equiv 0, \tag{7}$$

while the hemisphere surface becomes a floating potential to be solved. Otherwise were the potential at infinity held at ground as in most conventions, both the potential on the assumed hemisphere and the electrode become variables to be solved, which complicates the implementation of the double layer capacitance (and also Faradaic currents in future studies). After the simulation, the potential at infinity is then calculated as

$$\phi_{\infty}(t) = \phi(r,z,t)|_{\sqrt{r^2+z^2}=20a} - I(t)\cdot R_{rem}. \tag{8}$$

C. Input Current Pulses

Simulation was repeated with current input of the ordinary step input and the edge-retarded step input, respectively. Monophasic and more realistic biphasic stimulations could be easily calculated utilizing the linearity of the system. As a preliminary exploration, a ramp function is used to retard the leading edge of the pulse (Fig. 2). Without loss of generality, the length of transition was set equal to τ. Both current pulses reach the same amplitude ΔI.

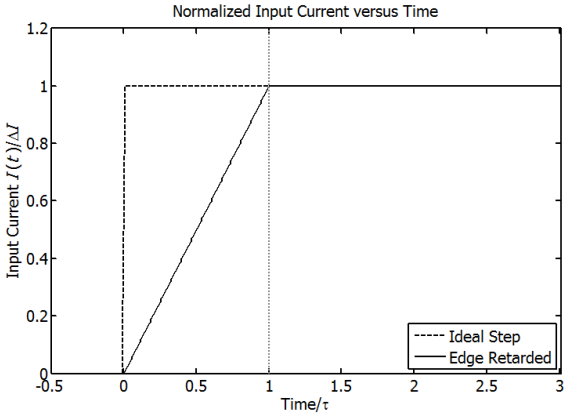

Figure 2. Input currents: ideal step function and modified step with rising edge retarded by a ramp. Dashed line indicates end of transition zone.

D. System Solving and Data Presenting

To accurately solve the equations at the disk edge, the time steps are chosen based on the spatial resolution [9]. Increments in time are 1/500 of the lumped circuit time constant τ from pulse start to $\tau/2$ after. This is about one eighth of the initial local time constant at $r = a - a/30000$ [7]. For the rest of the simulation the time steps are increased to $\tau/100$ to reduce computation. Data is output at time steps of $\tau/100$, processed with MATLAB R2010b (The MathWorks, Natick, MA).

For comparison with the theoretical calculation and other results, the reference point of the potentials in the presented data is shifted to the infinity point, while the current density values remain unchanged. Thus in all following data

$$V(r,z,t) = \phi(r,z,t) - \phi_{\infty}(t) \tag{9}$$

$$V_{metal}(t) = \phi_{metal}(t) - \phi_{\infty}(t), \tag{10}$$

where V denotes the shifted potential. For generality, the data are presented in dimensionless parameters e.g., time/τ and radius/a. Current density and potentials are normalized to corresponding parameters of the average geometric current density

$$J_0 = \Delta I/(\pi a^2) \tag{11}$$

and the theoretical initial voltage

$$\Delta V = \Delta I/(4\kappa a), \tag{12}$$

respectively. The theoretical initial voltage utilizes the same relationship from a voltage step problem, as initial conditions at the input onset are identical.

III. Results and Discussion

A. Current Density Profile and Current Nonuniformity

The normal current density at the disk surface $J_z(r,0,t)$ shows how the edge retarded input reduces the current edge enhancement of the electrode (Fig. 3, right). The overshoot above the average current density close to the edge is significantly smaller for the modified input, although at the pulse onset the current density would still theoretically reach infinity due to the singularity at the boundary of the disk.

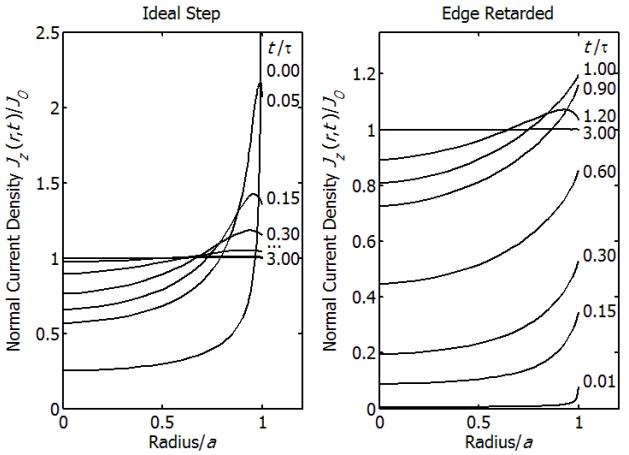

Figure 3. Current density profiles along radial axis at different time points. Edge enhancement beyond steady avereage is significantly reduced.

The current nonuniformity is evaluated with an area-weighted standard deviation from the geometric average value $J_{geom}(t)$:

$$\sigma_J(t) = \left[\frac{1}{\pi a^2}\int_0^a \left(J_z(r,0,t) - J_{geom}(t)\right)^2 2\pi r dr\right]^{\frac{1}{2}}. \quad (13)$$

To avoid the singularity at the edge of the disk electrode, the integral was performed up to $r = 0.9995a$ for numeric calculations. It shows that the nonuniformity diminishes as the current input pulse stays on (Fig. 4). The nonuniformity for the retarded input is not always smaller compared the step input, but this is mostly due to the fact that the modified input is still in transition while the step input has been redistribution charge along the radial direction since the pulse start. When the retarded input current reaches the steady state value ΔI, it has a smaller nonuniformity compared to the step input at the pulse beginning, therefore proving that its current enhancement above the steady state average is smaller.

Meanwhile the results of the step input provide verification (analysis not shown) with several previous studies for primary current profile, primary potential distribution, and effective lumped resistance [1], [2], as well as initial local time constant value [7]

$$\tau(r,0) = 2\tau\sqrt{1 - r^2/a^2}. \quad (14)$$

B. Charge and Potential Profiles

Charge density profiles could be calculated by the local double layer potential $V_{dl}(r,t)$:

$$\sigma(r,t) = \gamma V_{dl}(r,t) = \gamma\left(V_{metal}(t) - V(r,0,t)\right). \quad (15)$$

Fig. 5 reveals that though the current periphery enhancement is reduced by input edge-retarding, the charge accumulation still exhibits the same enhancement due to the integration of nonuniformity over time as well as charge relaxation along the radial direction. Charge density accumulation is slower for the retarded input as expected.

Fig. 6 shows that potential profiles in the two situations exhibit the identical asymptotic behavior reaching the same steady state, which is expected from the analytical studies of [3]. However they follow different time courses towards this asymptote starting from different initial conditions.

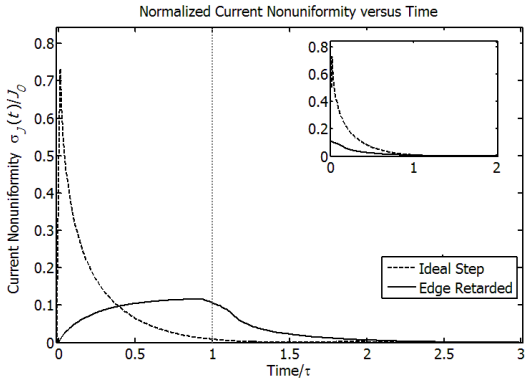

Figure 4. Current nonuniformity versus time. The decay of nonuniformity of the edge retarded input starts at smaller value when the input reachesΔI, and decays faster if properly aligned as seen in the inset.

C. Quantification of Edge Enhancement

Two quantities are calculated to compare current density enhancement above the average current density at steady state. The maximal current density at any given time is analyzed. Since comparison of infinity at the singularity is meaningless, a small annular region of the edge is excluded and the analysis is performed over the region of $r \le 0.9995a$. The normalized maximal current density against time is plotted in Fig. 7. For the modified current input, the maximum current density captured is only about 20% more than steady state average value, while the original one resulted in an almost tenfold overshoot before decaying to the average value.

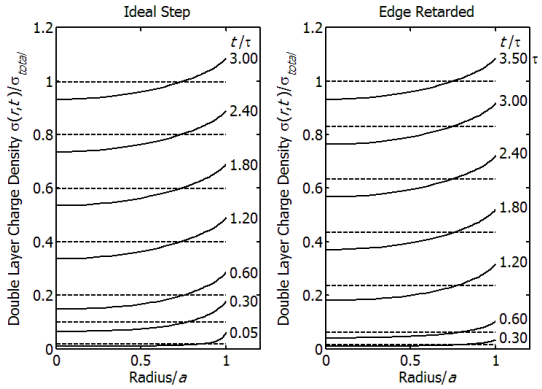

Figure 5. Double layer charge profile along radial axis at different time points. For side to side comparison, normalization on both sides utilize the average total charge density at 3τ for the ideal step input

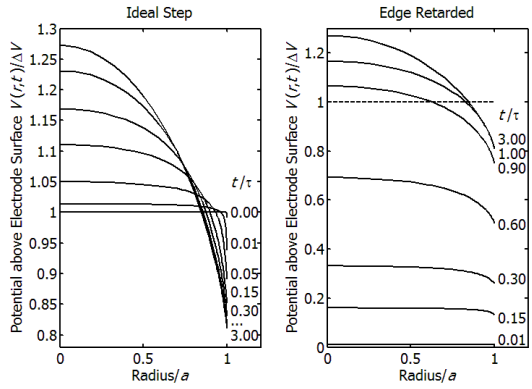

Figure 6. Potential profiles along radial axis at different time points, showing the same asymptotic distribution.

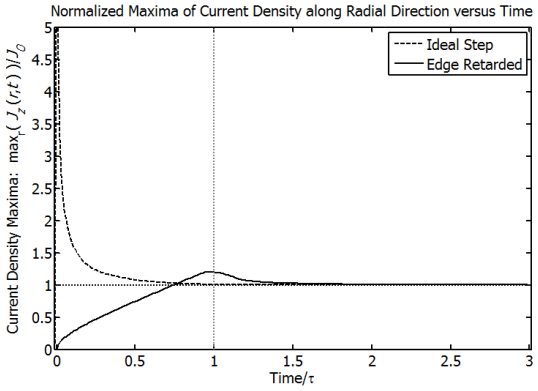

Figure 7. Current density maxima versus time.

The area-weighted average of surplus current density compared to steady state average value is also calculated and normalized to present how much current exceeds the desired uniform distribution. This dimensionless value is defined as the current overload index (COI)

$$COI(t) = \frac{1}{\Delta I}\int_{\{r|J_z(r,0,t)>J_0\}}(J_z(r,0,t) - J_0)2\pi r dr. \quad (16)$$

Accumulated COI could give an estimate of how much damage would be caused by the edge enhancement if average current density were to be set to the safety limits of the electrode. The accumulated value of *COI* (integral over normalized time) for the current step without and with edge retardation is 0.0593 and 0.0219, respectively, giving an almost threefold decrease. Fig. 8 shows that the edge retarded input has some current overloading at the transition from the rising phase to steady state, which is much smaller compared to that of the unmodified input. A more comprehensive analysis could also include the corrosion or other damage as a function of the current overload into the weight for this calculation, which is not discussed here.

D. Effect on Charge Injection Effectiveness

To minimize edge effects throughout the entire pulse, a transition zone should be added at the beginning and end of the pulse, since edge enhancement is noted at pulse offset as well. The total charge injection would remain the same for the edge retarded pulse, only increasing the overall pulse width. However less charge is injected with the modified current input at any given time after pulse onset compared to a rectangular pulse. The delay induced in invoking a desired effect would depend on how long a transition zone is applied. If the pulse width is relatively long compared to the transition zone, then the difference in charge injection at pulse end of the unmodified input is small and no significant delay in response or increase in stimulation threshold should be noticed.

IV. Conclusion

The results yield increased understanding of the effect of edge-retarding of current pulses on reducing edge enhancement of current density in disk electrodes. This provides a potential solution to the long-standing problem which would lie within the driving circuit rather than the electrodes themselves. This could utilize the natural behavior of current pulse generator, which will not have an ideally sharp step due to the limitation in circuit design as well as their load. Implementation could also be achieved through software programming rather than hardware manufacturing, and is therefore less complicated and easier to implement. The trade-off to pay could be charge injection efficiency or a delay in the system that is equal to the transition time. It should not to be an issue usually, unless very short pulses are required or the system is very time sensitive. This study provides the basis for future work to further study other edge-retarding waveforms with varying transition times in neural stimulation and other biomedical applications. Faradaic impedance and other aspects of the electrodes could be included in the model to obtain more realistic results.

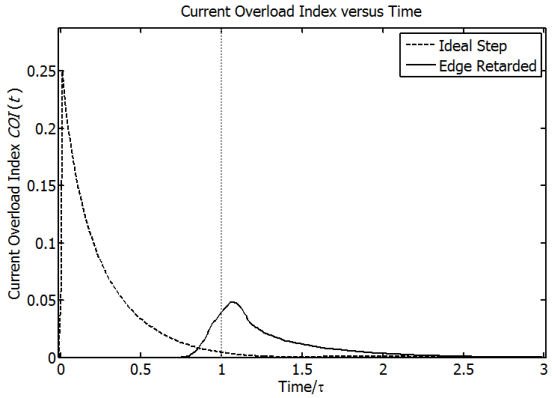

Figure 8. Current overload index versus time.

Acknowledgment

This work was supported by ERC (BMES).

References

[1] J. Newman, "Resistance for flow of current to a disk", *J. Electrochem. Soc.*, vol. 113, 1966, pp. 501–2.

[2] J. Newman. "Frequency Dispersion in Capacity Measurements at a Disk Electrode", *J. Electrochem. Soc.*, vol. 117, 1970, pp. 198

[3] J. Newman. "The Transient Response of a Disk Electrode", J. Electrochem., Soc., vol. 120, 1973, pp. 1339

[4] J. D. Wiley and J. G. Webster, "Analysis and control of the current distribution under circular dispersive electrodes," *IEEE Trans. Biomed. Eng.*, vol. BME-29, 1982, pp. 381–389.

[5] D. A. Ksienski, "A minimum profile uniform current density electrode," *IEEE Trans. Biomed. Eng.*, vol. 39, 1992, pp. 682–692.

[6] M. F. Suesserman, F. A. Spelman, J. T. Rubinstein, "In Vitro Measurement and Characterization of Current Density Profiles Produced by Nonrecessed, Simple Recessed, and Radially Varying Recessed Stimulating Eletrodes", *IEEE Trans. Biomed. Eng.*, vol. 38 1991, pp. 4104.

[7] K. B. Oldham, "The RC time constant at a disk electrode," *Electrochem. Commun.,* vol. 6, 2004, pp. 210–214.

[8] J. C. Myland and K. B. Oldham, "How does the double layer at a disk electrode charge?", *J. Electroanalyt. Chem.*, vol. 575, 2005, pp. 81–93.

[9] M. R. Behrend, A. K. Ahuja, and J. D. Weiland Dynamic Current Density of the Disk Electrode Double-Layer. *IEEE Trans. Biomed. Eng., v*ol.55-3, 2008, pp. 1056-1062.

[10] D. R. Cantrell and J. B Troy, "A Time Domain Finite Element Model of Extracellular Neural Stimulation Predicts that Non-Rectangular Stimulus Waveforms May Offer Safety Benefits", in *IEEE-EMBS Annual Meeting Conference Proceedings*, Vancouver, BC, Canada, 2008.

[11] D. R. Cantrell and J. B Troy, "Extracellular Stimulation of Mouse Retinal Ganglion Cells with Non-Rectangular Voltage-Controlled Waveforms", in *IEEE-EMBS Annual Meeting Conference Proceedings*, Minneapolis, MN, USA, 2009.